Element-Specific Magnetic Hysteresis of Individual 18 nm Fe Nanocubes

ARTICLE *in* NANO LETTERS · MARCH 2011

Impact Factor: 13.59 · DOI: 10.1021/nl200242c · Source: PubMed

NANO LETTERS

LETTER

pubs.acs.org/NanoLett

Element-Specific Magnetic Hysteresis of Individual 18 nm Fe Nanocubes

Florian Kronast,[†] Nina Friedenberger,[‡] Katharina Ollefs,[‡] Sebastian Gliga,[∥] Logane Tati-Bismaths,[⊥] Ronja Thies,[†] Andreas Ney,[‡] Ramona Weber,[†] Christoph Hassel,[‡] Florian M. Römer,[‡] Anastasia V. Trunova,[‡] Christian Wirtz,[‡] Riccardo Hertel,[§] Hermann A. Dürr,[#] and Michael Farle*[,‡]

[†]Helmholtz Zentrum Berlin für Materialien und Energie, Albert-Einstein-Strasse 15, 12489 Berlin, Germany

[‡]Fakultät für Physik and Center for NanoIntegration (CeNIDE), Universität Duisburg-Essen, Lotharstrasse 1, 47048 Duisburg, Germany

[§]Institut de Physique et Chimie des Matériaux de Strasbourg Université de Strasbourg, CNRS UMR 7504, 23 rue du Loess, 67034 Strasbourg Cedex 2 BP 43, France

[∥]Center for Nanoscale Materials, Argonne National Laboratory, Argonne, Illinois 60439, United States

[⊥]Institut für Experimentalphysik, Freie Universität Berlin, Arminallee 14, 14195 Berlin, Germany

[#]PULSE Institute, SLAC National Accelerator Laboratory, Menlo Park, California 94025, United States

Supporting Information

ABSTRACT: Correlating the electronic structure and magnetic response with the morphology and crystal structure of the same single ferromagnetic nanoparticle has been up to now an unresolved challenge. Here, we present measurements of the element-specific electronic structure and magnetic response as a function of magnetic field amplitude and orientation for chemically synthesized single Fe nanocubes with 18 nm edge length. Magnetic states and interactions of monomers, dimers, and trimers are analyzed by X-ray photoemission electron microscopy for different particle arrangements. The element-specific electronic structure can be probed and correlated with the changes of magnetic properties. This approach opens new possibilities for a deeper understanding of the collective response of magnetic nanohybrids in multifunctional materials and in nanomagnetic colloidal suspensions used in biomedical and engineering technologies.

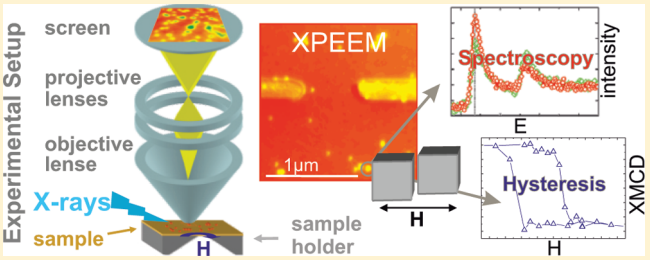

KEYWORDS: Nanoparticle, iron, magnetic, hysteresis, cubic, spectroscopy

Magnetic nanoparticles find manifold applications ranging from biomedicine over magnetic sensors to storage devices. The magnetic anisotropy energy density (MAE)[1] is the key material parameter to control the magnetic hardness, which is given by the coercive field and it strongly influences the thermal stability of individual ferro- or superparamagnetic nanoparticles. Depending on the application the thermal stability of the magnetization is desired to be high (10 years for data storage) or low (milliseconds for medical applications at room temperature). This time scale, that is, the superparamagnetic limit, can be tuned by the MAE and the volume of the particle. For example, by increasing the MAE the magnetic stability at room temperature can be changed by orders of magnitude to smaller particle sizes.[2] In general, the superparamagnetic limit can be determined by measuring the blocking temperature (T_B) below which the magnetization is considered to be stable over the time scale of the measurement. In nanoparticle ensembles, however, T_B is an average quantity and depends on the magnetic volume, the MAE, and the magnetic dipolar coupling of the individual particles. These quantities vary from particle to particle, for example, due to surface effects resulting from slightly different morphologies. Magnetic dipolar interactions depend on the orientation and magnitude of the temperature-dependent magnetization of the particles, the distance between them and their arrangement, making a determination of their individual magnetic parameters in ensemble measurements impossible. Experiments have shown for example, that different particle configurations in macroscopic ensembles can cause opposite shifts of T_B[3] which has been modeled[4] in terms of different magnetically coupled particle configurations. An experimental study correlating observed particle configurations with the magnetic macroscopic response has not yet been performed to the best of our knowledge.

Here, we experimentally address this challenge and determine the magnetization reversal behavior, i.e., the magnetic hysteresis, coercive fields, and magnetization of size-selected individual Fe nanocubes in different local configurations, that is, monomers, dimers, trimers, and other configurations at room temperature.

Received: January 21, 2011
Revised: February 18, 2011
Published: March 10, 2011

The magnetic characterization is correlated with a detailed imaging of the orientation, crystalline structure, chemical composition, and morphology of the individual cubes. The coercive field and the shape of the single particle hysteresis loops recorded for different orientations of the magnetic field provide a direct measure of the MAE which is analyzed within the framework of the Stoner−Wohlfarth theory of coherent reversal of the magnetization[5] in single domain nanomagnets. Summing over all the locally resolved hysteresis loops allows developing an understanding of the macroscopic collective magnetic response.

Ballistic Hall micromagnetometry,[6] differential phase contrast microscopy, holography, and energy-loss magnetic chiral dichroism in the transmission electron microscope (TEM)[7,8910] have been used to determine magnetic hysteresis and domain configurations for nanomagnets in the range between 30 nm[8] and 1 μm.[7] First experiments to measure the switching field, but not a full hysteresis loop, at low temperatures (35 mK < T < 30 K) of 20 nm Co nanoparticles embedded in Nb have been reported using a micro-SQUID technique.[11,12] Also, a bolometer detection scheme to record the static and high-frequency dynamic magnetic response of individual <10 nm colloidal nanoparticles with a moment of $\sim 10^5$ μ_B has been proposed.[13] All of these unique techniques require a highly specialized or complicated sample preparation, and only very few nanoparticles from a macroscopic batch can be analyzed in a reasonable amount of time, resulting in poor statistics. Due to the incompatibility of the above-mentioned experimental techniques the one-on-one correlation between crystal structure, composition, and morphology on the one hand and the electronic and magnetic structure on the other hand has not been possible for the same particle by in situ simultaneous analysis.

Recent developments in magnetic imaging by soft X-ray spectroscopies[14] like X-ray holography,[15] and (scanning) transmission X-ray microscopy[16−19] offer new possibilities with a claimed lateral resolution of about 25 nm. Element-specific imaging of the magnetic domain structure of continuous ferromagnetic layers has been demonstrated at resolutions of at best 50 nm. In pioneering work the size-dependent spin structure of Fe cluster ensembles prepared by a gas-phase cluster source and exchange coupled to a ferromagnetic Co substrate has been analyzed by X-ray photoemission electron microscopy (XPEEM) in combination with atomic force microscopy.[20−22] However, the determination of the MAE and the magnetic moment from hysteresis loops of single colloidal nanoparticles with dimensions smaller than 30 nm, which can be controllably prepared in the form of rods, platelets, or cubes and which have been structurally, morphologically, and chemically characterized with near atomic resolution[23,24] and reasonable statistics, remained a challenge.

Here, we show that XPEEM in combination with scanning electron microscopy (SEM)[20] can *simultaneously* provide quantitative information on the chemical state, coercive field, and magnetic moment[25,26] of hundreds of sub-20-nm individual nanomagnets in different configurations and in magnetic fields of up to 33 mT[27] in a single experimental run (!). While SEM is used to identify shape, geometry, orientation, and topological distribution, TEM is used to determine the crystalline structure and elemental composition. XPEEM allows the quantitative, element-specific determination of electronic structure, chemical state, and the orientation and magnitude of the magnetic moment including its spin and orbital contribution.

Eighteen nanometer Fe nanoparticles with a cubic shape were synthesized by organometallic synthesis as described earlier.[28]

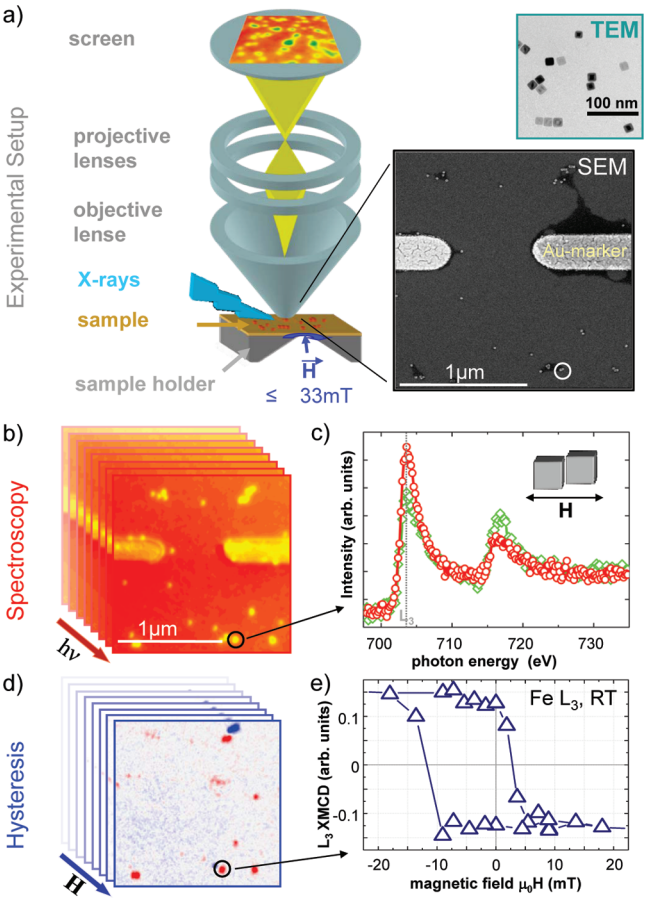

Figure 1. Magnetic imaging and spectromicroscopy of individual Fe nanocubes in an applied magnetic field of up to ±33 mT. (a, left) Schematics of the photoemission electron microscope with a magnetic yoke integrated into its sample holder. (a, right) Representative SEM image of a sample with Au markers and as-prepared Fe nanocubes and transmission electron microscopy image showing typical configurations of the nanocubes. (b) XPEEM image stacks of the same area at different photon energies $h\nu$ and (d) magnetic contrast at the Fe L_3 edge as a function of external magnetic field **H** applied along the indicated direction. Blue and red color indicate opposite magnetization directions in the particles. (c) X-ray absorption spectrum of one dimer (two Fe cubes aligned parallel to **H**) marked by the circles in images a, b, and d. Green diamonds correspond to positive and red circles to negative helicity of the photon. (e) A hysteresis loop for a dimer aligned with its easy axis parallel to the applied field recorded at the Fe L_3 edge (indicated by the dotted line in c).

The colloidal nanoparticles which are surrounded by an oxide shell and organic ligands were dispersed on a Si(110) substrate. Different configurations are obtained ranging from single nanocubes to dimers, trimers, and more complex configurations with a minimum distance between particles of ∼2 nm (Figure 1a) due to the hydrocarbon ligands. To obtain metallic, oxide-free Fe nanocubes for the magnetic characterization, the residual oxides and organic ligands were reduced by a plasma etching technique[35] which leaves the position of the particles unchanged.[29] Finally we protected the samples in situ by a thin Al layer against reoxidation.

In our experimental runs we simultaneously recorded several hundred magnetic hysteresis loops for different configurations of 18 nm Fe cubes (visible in the field of view of the XPEEM setup, Figure 1) relative to an applied magnetic field under identical

dx.doi.org/10.1021/nl200242c |*Nano Lett.* 2011, 11, 1710–1715

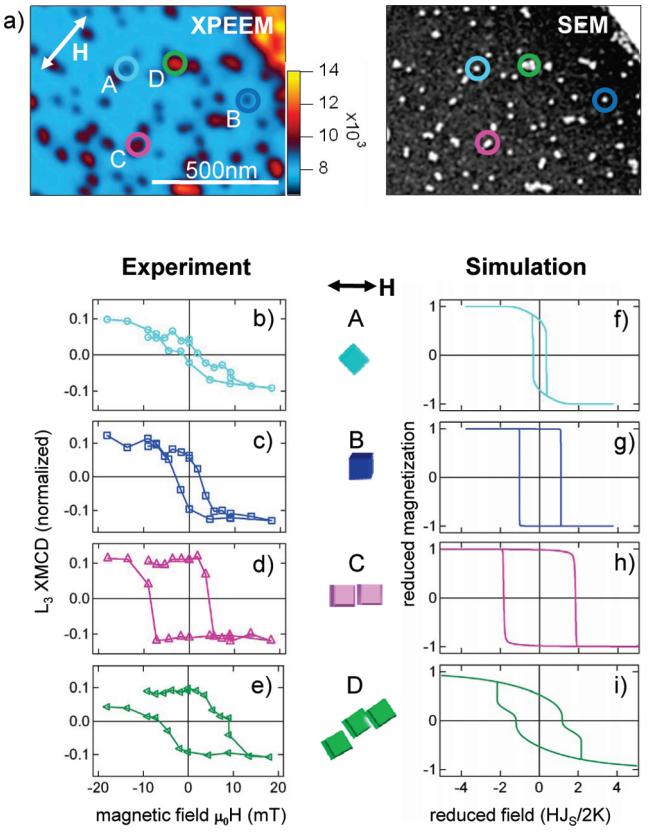

Figure 2. (a) Chemical contrast XPEEM image (left) at the Fe edge and SEM image of the same area (right). (b−e) Field-dependent magnetization of differently coordinated Fe nanocubes marked in (a). (f−i) Micromagnetic simulations of the configurations depicted in A to D with respect to the direction of the indicated magnetic field **H**. The magnetic field is normalized with respect to the anisotropy field $2K/J_S$ ($J_S = \mu_0 M_s$, M_s; magnetization).

conditions at 300 K. This approach allows correlating the magnetic responses, the influence of anisotropies, and dipolar interactions of local configurations and particle states with macroscopic measurements, as well as to observe changes of the electronic structure due to changes of the chemical state induced, e.g., by controlled chemisorption or ligand exchange. Selected experimental loops at 300 K will be compared here to micromagnetic simulations (for details see Methods).

For our experiments we used the XPEEM setup at the Berlin Synchrotron facility BESSY II schematically shown in Figure 1a. The oxidation state and the magnetic spin moments of the Fe nanocubes were determined from spectra and hysteresis loops like the ones shown in panels c and e of Figure 1 and Figure 2. The local coordination and orientation of the cubes were determined from TEM and SEM images as shown in Figure 1a on the right. The corresponding chemical and magnetic contrast image series (Figure 1b,d) were determined by means of spectromicroscopy at the L_3 edge of Fe.[30] The image series in Figure 1b was recorded as a function of photon energy between 690 and 740 eV for the L_3 and L_2 edges of Fe. Each pixel of the image series yields an X-ray absorption spectrum (XAS) with a lateral resolution of about 20 nm. In Figure 1d, the sequence of images of the same sample area which show the magnitude of the dichroic signal in false colors as explained in the Supporting Information is shown. The dichroic signal yields the magnetic moment per atom. Hysteresis loops of different particle configurations were extracted by plotting the magnetic (dichroic) signal at the Fe L_3 edge for each pixel or collection of pixels (Figure 1d) as a function of the magnetic field. An example for a spatially resolved hysteresis loop of a typical dimer configuration consisting of two Fe nanocubes oriented with the {100} facets facing each other (marked with a circle in Figure 1b, d and the SEM image of Figure 1a) is shown in Figure 1e. A movie showing the field-dependent changes of the XPEEM images and associated hysteresis loops can be found in the Supporting Information.

The Fe cubes show no evidence of oxidation within the probing depth of 5−7 nm. The magnetic moment per Fe atom of the dimer configuration was determined in the saturated state with the magnetic field $\mu_0 H_{max} = -20$ mT applied parallel to the dimer axis (Figure 1c,e). Using the sum rules[31,32] of XMCD and assuming the bulklike number of Fe d-holes $n_{3d} = 3.39$,[26] we calculate a bulklike $\mu_l/\mu_s = 0.072 \pm 0.03$ and a spin magnetic moment per Fe atom $\mu_s = 1.17 \pm 0.2\ \mu_B$ which is about half the bulk value of body-centered cubic (bcc) Fe. This apparent reduction is most likely due to thermal fluctuations of the particle's magnetization over the acquisition time of the ten averaged spectra (~200 min), that is a slow superparamagnetic response, at room temperature. From micromagnetic simulations we can exclude noncollinear spin alignments at the surfaces of the particles as the origin of the strongly reduced magnetization. Such a spin canting would be in the range of a few degrees only, leading at most to a decrease of the magnetization of less than 1%. The Al capping and the resulting alloy formation of Al and Fe at the interface is not likely to explain the reduction of the Fe magnetic moment μ_{Fe} either. For disordered $Fe_{1-x}Al_x$ alloys μ_{Fe} is reduced to ~0.9 μ_B and ~0.2 μ_B for FeAl and $FeAl_3$.[33] Taking into account our probing depth of 5−7 nm, an at least 4 nm thick intermixed interface would be necessary which is substantially larger than the 0.6 nm Fe/Al interlayer thickness found for thin films.[34] A 30% reduced saturation magnetization had also been reported for an ensemble of similar Fe nanocubes.[35] Even assuming that each Fe cube contains 10% of an antiferromagetic Fe oxide could not explain this reduction. Consequently, the reduced magnetic moment of our nanocubes cannot be explained by a partial oxidation either.

Figure 2 shows examples of magnetic hysteresis loops of single cubes (b and c), a dimer (d), and one trimer (e) configuration with respect to different orientations of the applied magnetic field *H*. The positions of the corresponding particles are indicated by the respective colors in the XPEEM and SEM images of Figure 2a. The Fe L_3 XMCD signal is normalized and proportional to the average magnetic moment per Fe atom in each configuration. In general, the experimental spectra of different cube configurations reveal either superparamagnetic or ferromagnetic behavior at room temperature without any obvious difference in the chemical composition. For individual Fe nanocubes we find the expected dependence of the hysteresis loops on the orientation of the applied magnetic field (Figure 2b, c) indicating an easy axis of the magnetization along a ⟨100⟩ direction (cube edge) and a magnetically hard direction along the ⟨110⟩ direction of the Fe cube. The coercive fields $\mu_0 H_C \sim 2$mT are much smaller than the ones calculated in Figure 2f, g by micromagnetic simulations[36] using bcc bulk Fe parameters. As mentioned above, this is most likely due to instabilities of the magnetization over the time scale of the measurement and the fact that the system is close to the superparamagnetic limit. Indeed, for a Fe cube of ~18 nm side length with bulklike

dx.doi.org/10.1021/nl200242c |*Nano Lett.* 2011, 11, 1710–1715

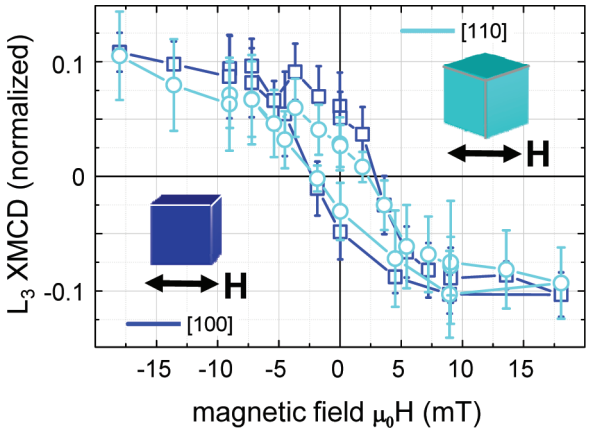

Figure 3. Averaged hysteresis loops of about 100 single nanocubes recorded with the magnetic field oriented parallel to the cube edge (⟨100⟩) or at angle of 45° (⟨110⟩). The rounding in comparison to Figure 2 is due to the fact that loops of cubes which were oriented within ±22° with respect to the magnetic field direction were also averaged.

MAE and reduced magnetization, one estimates a T_B close to the measuring temperature of 300 K. Qualitative differences in the shape and remanent magnetization between the hysteresis loops (Figure 2b,c) correspond rather nicely to the simulated ones. A much better quantitative agreement can be achieved when one considers the atomically rough topography of the Fe cubes and the small deviations from perfect cubic symmetry evident also in the TEM images of Figure 1a and the Supporting Information.

To confirm the orientation of the easy axis of magnetization in the nanocubes, in general, we analyzed the orientations using high-resolution SEM images and hysteresis loops of nearly ∼100 nanocubes. Half of the hysteresis loops were obtained for particles with the edge axis parallel to the applied magnetic field, the other half for H applied at an angle of 45°. In the averaged hysteresis loops shown in Figure 3 blue squares represent the loop for cubes oriented with their ⟨100⟩ axis along the magnetic field direction while circles represent the one for cubes oriented with the ⟨110⟩ axis along the magnetic field direction. The enhanced remanence in the hysteresis recorded with the magnetic field along the ⟨100⟩ axis gives clear evidence for the presence of magnetocrystalline anisotropy with a preferred magnetization along the ⟨100⟩ axis as confirmed by our micromagnetic simulations shown in Figure 2f,g. The two average loops shown in Figure 3 resemble the loops of a macroscopic measurement which masks the influence of small variations in particle size and orientation and averages over small changes of MAE from particle to particle.

For the dimer and trimer (Figure 2d,e) and also for other more complex configurations (not shown here), we find large variations in the coercive field and the shape of the hysteresis loops which can be qualitatively understood by micromagnetic simulations (Figure 2h,i) again assuming bulk Fe parameters at 300 K. The dimer configuration (C in Figure 2) consists of two nanocubes arranged face to face with adjacent {100} planes. The long axis of the dimer was oriented along the axis of the magnetic field. Its magnetic response in Figure 2d shows a wide open rectangular hysteresis. The enhanced coercive field (∼7.5 mT) and the 100% remanence at zero field demonstrate the contribution of magnetic dipolar coupling between the neighboring Fe nanocubes. Obviously, the dipolar coupling enhances the shape anisotropy and stabilizes the magnetization of the dimer resulting in a higher blocking temperature. This explanation is confirmed by our micromagnetic calculations (Figure 2h) showing an increased H_C. The experimental hysteresis shows an unexpected horizontal shift to negative fields reminiscent of the exchange bias effect[37,38] usually due to the unidirectional coupling between an antiferromagnet and a ferromagnet. This horizontal shift is observed only for dimer or linear trimer configurations, not for single particles. In configurations of several closed packed nanocubes this shift is very small or not detectable. The origin of this peculiar "exchange bias" is not clear. An antiferromagnetic material is not apparent in our sample. FeAl alloys have shown antiferromagnetic correlations which might be a possible route for explanation. However, the existence of an intermixed antiferromagnetic FeAl interface layer cannot be the explanation, since the "exchange bias" should also be present for single particles. Also, the trivial effect of an apparent shift due to the contributions of magnetic stray fields from other nanocubes can be ruled out for the dimers discussed here. According to our micromagnetic simulations the stray field of the Fe nanocubes (assuming full bulklike magnetization) is smaller than 2 mT at a distance of approximately 60 nm. As a result, we have to consider either a complex unidirectional coupling due to diverging stray fields at the cube edges or the presence of an antiferromagnetic bottom layer (e.g., α-Fe_2O_3) which cannot be completely ruled out. While the latter should also be present in monomers, the complex stray field coupling could be present only in specially ordered dimers or polymers. However, at the current status of our simulations this complex situation involving a strongly inhomogeneous magnetization per cube cannot be interpreted at present and requires further investigation.

In Figure 2e the magnetization curve of a trimer (D) with the magnetic field oriented as indicated in the figure is shown. This configuration shows an interesting two-step magnetization reversal which is also seen for other, slightly different configurations of trimers. In our micromagnetic simulations (Figure 2i) in which one nanocube is not aligned face-to-face but includes some angle with the other two nanocubes (D), we find a similar behavior. Compared to the dimer in Figure 2d this configuration has a significantly reduced saturation magnetization. This points to the presence of magnetic fluctuations or frustration, caused by the larger distance between the Fe nanocubes or their noncollinear alignment, respectively. Unfortunately we cannot resolve this particular configuration. Nevertheless the measured hysteresis demonstrates the complexity of magnetic coupling in configurations of more than two Fe nanocubes which can only be addressed with the appropriate spatial resolution and specific contrast. Instrumental developments such as aberration corrected PEEM[39] promise a much more detailed insight into the magnetic properties of individual nanomagnets in the near future, making additional SEM images dispensable. Furthermore, element-specific studies on individual bimetallic, complex nanomagnets, e.g., core−shell nanoobjects with unconventional, nonaligned spin configuration will become feasible.

In conclusion, we present an element-specific study of single nanoparticle magnetic properties and their interactions in complex particle arrangements. We show single particle magnetization curves of 18 nm Fe nanocubes in different orientations. Comparing our experimental data to micromagnetic simulations, we can identify the influence of dipolar coupling and intrinsic magnetic anisotropy on the magnetic response. We find that

dx.doi.org/10.1021/nl200242c |*Nano Lett.* 2011, 11, 1710–1715

magnetic dipolar coupling between neighboring nanocubes increases the coercive fields and stabilizes the magnetization. An unusual horizontal shift of the hysteresis loops of dimers is detected which cannot be explained by a conventional exchange bias effect. Our experimental approach opens up new possibilities for a more detailed understanding of the single and collective behavior of magnetic nanoparticles, a knowledge that is also of importance for modern engineering and biomedical applications.

Methods. *Experimental Setup and Performance.* The XPEEM instrument is based on a commercial Elmitec photoemission electron microscope attached to a soft X-ray microfocus beamline (UE49) with 10 × 15 μm spot size and full polarization control. With X-ray excitation the microscope provides a spatial resolution of 25 nm. The XPEEM image in Figure 1b demonstrates that this resolution is sufficient to resolve individual Fe nanocubes. Additional information about nanoparticle sizes and their local orientation can be extracted from previously taken high-resolution scanning electron microscopy images (SEM) also shown in Figure 1a. We use a grid of lithographically prepared Au markers to identify the same sample position in PEEM and SEM and match those SEM images to our PEEM data.

X-ray absorption spectra were obtained by reading out the intensity at the particle position as a function of photon energy out of an image stack where each image was recorded at 0.2 eV different photon energy (Figure 1b). Background normalization was performed by using a surrounding region containing no particle.

A sample holder with integrated magnetic yoke was used to apply magnetic fields of up to 33 mT during imaging.[27] Recording a stack of images during a magnetic field sweep allows us to extract the hysteresis of almost any nanoparticle configuration within our field of view.

To measure the hysteresis of individual Fe nanocubes we tuned the photon energy to the Fe L_3 edge (indicated by the line in Figure 1c and recorded series of PEEM images with circular polarization and alternating photon helicity (90% degree of polarization). To improve statistics we took about 600 images (1 s exposure time) at each field. Images were corrected for drift and coadded for each magnetic field and helicity.

Finally, we integrated the intensity from a particular region of interest containing an individual particle or cluster to calculate the corresponding XMCD signal. A neighboring region of interest containing no particle was used to perform a local background subtraction. The X-ray magnetic circular dichrosim is displayed as the difference of Fe L_3 intensities for two opposite helicities divided by their sum. Therefore the amplitude of the magnetic signal is not related to the visibility of an individual nanoparticle but only to its magnetic alignment. We are sensitive to the component of the magnetization vector **M** parallel or antiparallel to the wave vector **k** of the incident X-ray beam. The later differs from the direction of the applied magnetic field **H** by the grazing incidence angle of 16°.

Micromagnetic Simulations. Micromagnetic simulations were performed using a proprietary finite-element code solving the Landau−Lifshitz−Gilbert equation in three-dimensional samples. The most frequently used approach to simulate hysteresis loops with micromagnetic codes is the stepwise reduction or increase of the external field once an energetic minimum is reached. In our simulations we have chosen a different method which consists in a linear variation of the external field in time. This approach can suppress fast magnetic precession processes and other artifacts that may occur from the stepwise change of the field. The hysteresis loops were determined in the quasi-static limit; i.e., the external field was swept slowly enough to ensure that the magnetic system remains at any time very close to the energy minimum. Energy minimization was obtained by means of dynamic simulations with strong damping (Gilbert damping $\alpha = 0.5$), thereby ensuring that the magnetization remains close to the local effective field. The magnetostatic interaction, including the coupling between separate particles, is calculated using a hybrid finite-element/boundary element method. Each Fe cube was discretized into ca. 4400 tetrahedral elements, yielding an average cell size of 1.3 nm^3. The simulations were performed with the following material parameters for Fe: $A = 21$ pJ/m (exchange constant) and saturation magnetization $J_S = 2.15$ T.

■ ASSOCIATED CONTENT

Supporting Information. TEM and SEM images of Fe nanocubes with markers and a movie showing the field-dependent changes of the XPEEM images and associated hysteresis loops. This material is available free of charge via the Internet at http://pubs.acs.org.

■ AUTHOR INFORMATION

Corresponding Author

*E-mail: farle@uni-due.de.

Author Contributions

F.K., N.F., K.O., L.T.-B., and R.T. performed the experiments. F.K., N.F., L.T.-B., R.W., and R.T. evaluated the data. N.F., C.H., F.M. R., A.V.T., C. W., K.O., and A. N. prepared the samples. S.G. and R.H. performed the micromagnetic calculations. F.K., N.F., and M.F. prepared the manuscript with the contributions from all authors. M.F. and H. D. supervised the project.

■ ACKNOWLEDGMENT

Financial support by the DFG (SFB 445), the EC (MRTN-CT-2004-005567), and the "Helmholtz-Zentrum Berlin für Materialien und Energie GmbH (HZB)" is acknowledged. A.N. thanks the Heisenberg Programm of the DFG for support.

■ REFERENCES

(1) O'Handley, R. C. *Modern Magnetic Materials: Principles and Applications*; Wiley-VCH: New York, 1999.

(2) Sun, S.; Murray, C. B.; Weller, D.; Folks, L.; Moser, A. Monodisperse FePt Nanoparticles and Ferromagnetic FePt Nanocrystal Superlattices. *Science* **2000**, *287*, 1989–1992.

(3) Frandsen, C.; et al. Interparticle interactions in composites of nanoparticles of ferrimagnetic γ- Fe2 O3 and antiferromagnetic (CoO, NiO) materials. *Phys. Rev. B* **2004**, *70*, No. 134416.

(4) Berkov, D. V. Density of energy barriers in fine magnetic particle systems. *IEEE Trans. Magn.* **2002**, *38*, 2637–2639.

(5) Stoner, E. C.; Wohlfarth, E. P. A Mechanism of Magnetic Hysteresis in Heterogeneous Alloys. *Philos. Trans. R. Soc., A* **1948**, *240*, 599–642.

(6) Kuhn, L. T.; et al. Magnetisation of isolated single crystalline Fe-nanoparticles measured by a ballistic Hall micro-magnetometer. *Eur. Phys. J. D* **2000**, *10*, 259–263.

(7) Uhlig, T.; Zweck, J. Recording of single-particle hysteresis loops with differential phase contrast microscopy. *Ultramicroscopy* **2004**, *99*, 137–142.

(8) Snoeck, E.; Gatel, C.; Lacroix, L. M.; Blon, T.; Lachaize, S.; Carrey, J.; Respaud, M. Magnetic Configurations of 30 nm Iron Nanocubes Studied by Electron Holography. *Nano Lett.* **2008**, *8*, 4293–4298.

(9) Schattschneider, P.; et al. Detection of magnetic circular dichroism on the two-nanometer scale. *Phys. Rev. B* **2008**, *78*, No. 104413.
(10) Schattschneider, P.; et al. Detection of magnetic circular dichroism using a transmission electron microscope. *Nature* **2006**, *441*, 486–488.
(11) Thirion, C.; Wernsdorfer, W.; Mailly, D. Switching of magnetization by nonlinear resonance studied in single nanoparticles. *Nat. Mater.* **2003**, *2*, 524–527.
(12) Wernsdorfer, W.; Hasselbach, K.; Mailly, D.; Barbara, B.; Benoit, A.; Thomas, L.; Suran, G. Magnetization of single magnetic particles. *J. Magn. Magn. Mater.* **1995**, *140−144*, 389–390.
(13) Rod, I.; Kazakova, O.; Cox, D. C.; Spasova, M.; Farle, M. The route to single magnetic particle detection: a carbon nanotube decorated with a finite number of nanocubes. *Nanotechnology* **2009**, *20*, 335301.
(14) Dürr, H. A.; et al. A Closer Look Into Magnetism: Opportunities With Synchrotron Radiation. *IEEE Trans. Magn.* **2009**, *45*, 15–57.
(15) Eisebitt, S.; et al. Lensless imaging of magnetic nanostructures by X-ray spectro-holography. *Nature* **2004**, *432*, 885–888.
(16) Amaladass, E.; Ludescher, B.; Schütz, G.; Tyliszczak, T.; Eimüller, T. Size dependence in the magnetization reversal of Fe/Gd multilayers on self-assembled arrays of nanospheres. *Appl. Phys. Lett.* **2007**, *91*, No. 172514.
(17) Fischer, P.; et al. Element-specific imaging of magnetic domains at 25 nm spatial resolution using soft x-ray microscopy. *Rev. Sci. Instrum.* **2001**, *72*, 2322–2324.
(18) Im, M. -Y.; et al. Direct Real-Space Observation of Stochastic Behavior in Domain Nucleation Process on a Nanoscale. *Adv. Mater.* **2008**, *20*, 1750–1754.
(19) Kim, D.-Y.; et al. Magnetic soft x-ray microscopy at 15 nm resolution probing nanoscale local magnetic hysteresis (invited). *J. Appl. Phys.* **2006**, *99*, 08H303.
(20) Fraile Rodríguez, A.; Nolting, F.; Bansmann, J.; Kleibert, A.; Heyderman, L. J. X-ray imaging and spectroscopy of individual cobalt nanoparticles using photoemission electron microscopy. *J. Magn. Magn. Mater.* **2007**, *316*, 426–428.
(21) Bansmann, J.; et al. Magnetism of 3d transition metal nanoparticles on surfaces probed with synchrotron radiation—from ensembles towards individual objects. *Phys. Status Solidi B* **2010**, *247*, 1152–1160.
(22) Fraile Rodríguez, A.; et al. Size-dependent spin structures in iron nanoparticles. *Phys. Rev. Lett.* **2010**, *104*, No. 127201.
(23) Yacamán, J. M., Ascencio, J. A., Liu, H. B. & Gardea-Torresdey, J. Structure shape and stability of nanometric sized particles. *J. Vac. Sci. Techonol.* **2001**, *19*, 1091−1103
(24) Wang, R. M.; et al. Layer Resolved Structural Relaxation at the Surface of Magnetic FePt Icosahedral Nanoparticles. *Phys. Rev. Lett.* **2008**, *100*, No. 017205.
(25) Stöhr, J.; Padmore, H. A.; Anders, S.; Stammler, T.; Scheinfein, M. R. Principles of x-ray magnetic dichroism spectromicroscopy. *Surf. Rev. Lett.* **1998**, *5*, 1297–1308.
(26) Chen, C. T.; et al. Experimental confirmation of the x-ray magnetic circular dichroism sum rules for iron and cobalt. *Phys. Rev. Lett.* **1995**, *75*, 152–155.
(27) Kronast, F.; Schlichting, J.; Radu, F.; Mishra, S.; Noll, T.; Dürr, H. A. Spin resolved photoemission microscopy and magnetic imaging in applied magnetic fields. *Surf. Interface Anal.* **2010**, *42*, 1532–1536.
(28) Shavel, A.; Rodríguez-González, B.; Spasova, M.; Farle, M.; Liz-Marzán, L. M. Synthesis and Characterization of Iron/Iron Oxide Core/Shell Nanocubes. *Adv. Funct. Mater.* **2007**, *17*, 3870–3876.
(29) Wiedwald, U.; et al. From colloidal Co/CoO core/shell nanoparticles to arrays of metallic nanomagnets: Surface modification and magnetic properties. *ChemPhysChem* **2005**, *6*, 2522–2526.
(30) Kuch, W. X-ray magnetic circular dichroism for quantitative element-resolved magnetic microscopy. *Phys. Scr.* **2004**, *T109*, 89–95.
(31) Thole, B. T.; Carra, P.; Sette, F.; van der Laan, G. X-ray circular dichroism as a probe of orbital magnetization. *Phys. Rev. Lett.* **1992**, *68*, 1943–1946.
(32) Carra, P.; Thole, B. T.; Altarelli, M.; Wang, X. X-ray circular dichroism and local magnetic fields. *Phys. Rev. Lett.* **1993**, *70*, 694–697.
(33) Booth, J. G. *Springer Materials—The Landolt-Börnstein Database*,Wijn, H. P. J., Ed., Fig. A103−A137.
(34) Egelhoff, J.,W.F.; et al. Surface oxidation as a diffusion barrier for Al deposited on ferromagnetic metals. *J. Appl. Phys.* **2001**, *89*, 5209–5214.
(35) Trunova, A. V.; et al. Magnetic characterization of iron nanocubes. *J. Appl. Phys.* **2008**, *104*, No. 093904.
(36) Hertel, R.; et al. Three-dimensional magnetic-flux-closure patterns in mesoscopic Fe islands. *Phys. Rev. B* **2005**, *72*, No. 214409.
(37) Meiklejohn, W. H.; Bean, C. P. New magnetic anisotropy. *Phys. Rev.* **1956**, *102*, 1413–1414.
(38) Nogués, J.; et al. Exchange bias in nanostructures. *Phys. Rep.* **2005**, *422*, 65–117.
(39) Fink, R.; et al. SMART: A planned ultrahigh-resolution spectromicroscope for Bessy II.. *J. Electron Spectrosc. Relat. Phenom.* **1997**, *84*, 231.